Analysis of the Structural Integrity of a Floating Semisubmersible Foundation for Offshore Wind

Diogo Rosário Dias
diogo.r.dias@tecnico.ulisboa.pt

Instituto Superior Técnico, Universidade de Lisboa, Portugal

November 2017

Abstract

Floating wind power is a promising solution to the expansion of offshore wind, as it can be used in deeper water as well as it allows the usage of large wind turbines. Nonetheless, this technology is still in demonstration, with just a few full-scale prototypes all over the world. On this thesis the structural integrity of a semisubmersible floating foundation for offshore wind is studied, which foundation was created within the DeepCwind consortium in order to validate aero-hydro-servo-elastic numerical codes. Thereby, the focus is on the development of an appropriate numerical model for the structural analysis of the foundation. FAST 8, an aero-hydro-servo-elastic numerical code, was used to obtain the various loads applied on the structure. These loads were preprocessed before their input on a finite element model developed using ANSYS software. A submodeling technique was used to analyse with more precision and detail the stress concentration regions of the structure. Static and transient structural analysis allowed to find critic regions of the foundation and hence begin an iterative reinforcement process, allowing the study of the structure's suitability for use in offshore environments. Moreover, a modal analysis and a hydrodynamic response analysis of both the original and reinforced structures were made and their results compared. Results show that the DeepCwind floating semisubmersible cannot stand the severe offshore environment it was designed to.

Keywords: offshore wind power, floating, semisubmersible, DeepCwind, structural analysis, finite elements, submodeling

1 INTRODUCTION

Offshore wind turbines are a leading renewable energy technology capable of supporting a low-carbon economy in world. The offshore wind industry relies essentially on fixed-base foundations such as monopiles, space frame jackets and tripods, whose use is limited to shallow waters, thereafter limiting the growth of this industry. Since floating offshore wind foundations are not limited by water depth, they are a solution with great prospect to unlock the full-potential of the offshore wind market [6].

A typical floating wind turbine comprises a rotor nacelle assembly, a tower, a foundation and a mooring system. Since they are floating structures, they have 6 DOF. According to Butterfield et al. [5], they can be classified by three main physical principles used to archive stability. Thus, Spar-type rely on ballasting, TLP count on the mooring lines tension, and semisubmersible makes use of the distributed buoyancy, taking advantage of the weighted water plane area. The latter is the case of the studied foundation, although it also uses ballasting as a secondary source of stability. In reality, all foundations achieve stability from the three presented principles, but rely in one as the main source.

The foundation subjected to analysis was the floating semisubmersible foundation examined in the OC4-project (Offshore Code Comparison Collaboration Continuation) whose design was originated from the activities of the DeepCwind consortium, in order to verify the floating capabilities of various aero-hydro-servo-elastic numerical codes [12, 20, 21]. This foundation uses the NREL 5 MW Reference wind turbine [19], described in Ref. [10].

Although multi-body formulations based on beam elements are a common practice [14], the use of shell elements allows for a more detailed modelling of structure [14]. Shell elements were used on a global model of the structure.

To model the loads on the foundation and mooring lines computational fluid dynamics models (CFD) can be used, as well as potential flow theories and Morison's equation, or even a hybrid model made of a combination of the latter two.

In agreement with GL guidelines for offshore wind power [1], various DLC (design load cases) have to be considered. Nevertheless, this analysis was based on DLC 1.1 to find critic regions and test alternative solutions.

2 MODEL DEFINITION

2.1. Foundation

The DeepCwind semisubmersible is made of three columns arranged in a triangular array (figure 1). They are responsible for the buoyancy and stability of the platform. These columns are made of two parts: the upper columns (UC) and the base columns (BC), the latter performing functions of heave plates. All member thicknesses and dimensions can be found in Ref. [19], as well as a detailed description of the remaining components and systems.

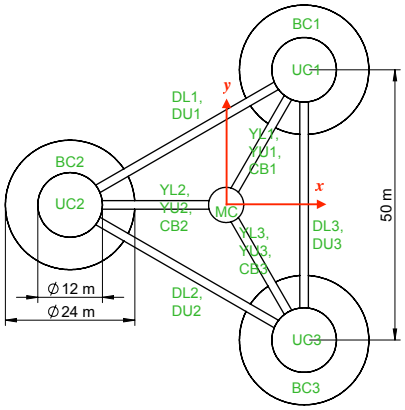

Figure 1: DeepCwind foundation top view with members captioned as in Ref. [19].

2.2. Hydrodynamic loads

The aero-hydro-servo-elastic numerical code FAST 8 was used to model the loads on the foundation, mooring lines, tower and rotor nacelle assembly, because the DeepCwind semisubmersible was already implemented on its *Certification Test 25*. For the case of floating structures, made of big dimension members, the use of potential flow theory is sometimes appropriate, as it accounts for diffraction and radiation effects [19]. On the other hand, when flow separation occurs, viscous-drag forces become dominant and the use of Morison's equation is preferable [19]. Among other factors, a proper formulation depends on the Keulegan-Carpenter number KC, and Reynolds number Re, defined by:

$$KC = \frac{uT}{D} \qquad (1) \qquad\qquad Re = uD/v \qquad (2)$$

where u is the is fluid velocity normal to the cylinder, T the wave period, D the diameter, and v is the fluid's kinematic viscosity [19]. Flow separation becomes important when $KC > 2$. Besides, the diameter to wavelength ratio D/λ is also an important factor to determine the proper formulation. If this ratio exceeds 0.2, diffraction effects are important. Hence, as KC increases and D/λ decreases with the increasing severity of wave conditions, Morison's equation is the preferred formulation for severe wave conditions. A detailed explanation on the subject, scoping the DeepCwind semisubmersible can be found in Ref. [19]. The most severe wave conditions are believed to be the most demanding from a structural point of view. For this reason, Morison's equation was used to compute the loads of the most demanding wave conditions within the DLC 1.1.

A Morison's equation only modelling approach requires the definition of the hydrodynamic coefficients of the submerged members. This coefficients, for transverse flow, are the drag coefficient C_d, the added-mass coefficient C_a, and the pressure coefficient C_p. Likewise, coefficients for axial flow are also defined, and noted with the subscript z. On Refs. [19, 21] the suitable hydrodynamic coefficients for the DeepCwind semisubmersible members are determined. Table 1 resumes the hydrodynamic coefficients used on the analysis. CFD analysis were not considered due to their high computational cost [14] and because FAST presented good accordance with other numerical codes as well as results from tank-tested scaled models .

Table 1: Hydrodynamic coefficients of the DeepCwind semisubmersible, according to [19, 21].

	C_d	C_{dz}	C_a	C_{az}	C_p	C_{pz}
MC	0.56	0	0.630	0	1	1
UC	0.61	0	0.630	0	1	0
BC $z = -14$	0.68	0	0.428	0	0.5	0
BC $z = -20$	0.68	9.6	1	0	1	1
Pontoons[1]	0.63	0	0.630	0	1	0

The total distributed hydrodynamic loads along the length of a member $\overrightarrow{F}$ for a Morison-only model is computed as: [13]

$$\begin{aligned}\overrightarrow{F} =& \overrightarrow{F}_{\mathrm{D}} + \overrightarrow{F}_{\mathrm{I}} + \cancel{\overrightarrow{F}}_{\mathrm{B}} + \overrightarrow{F}_{\mathrm{MG}} + \cancel{\overrightarrow{F}}_{\mathrm{F\,B}} + \dots \\ &+ \overrightarrow{F}_{\mathrm{AM}} + \overrightarrow{F}_{\mathrm{MG\,AM}} + \overrightarrow{F}_{\mathrm{F\,AM}}\end{aligned} \qquad (3)$$

where $\overrightarrow{F}_{\mathrm{D}}$ is the drag force, $\overrightarrow{F}_{\mathrm{I}}$ the inertia force, $\overrightarrow{F}_{\mathrm{B}}$ the buoyancy force, $\overrightarrow{F}_{\mathrm{MG}}$ the weight of the marine growth, $\overrightarrow{F}_{\mathrm{F\,B}}$ force due to fluid ballasting, $\overrightarrow{F}_{\mathrm{AM}}$ the added mass of the structure, $\overrightarrow{F}_{\mathrm{AM\,MG}}$ the added mass due to marine growth, $\overrightarrow{F}_{\mathrm{F\,AM}}$ the added mass due to fluid ballasting. A well documented description on how these terms are computed can be found on HydroDyn's Theory Manual [13] (HydroDyn is the FAST module respon-

[1] On this document *pontoons* refer to all the CB, YL, YU, DL and DU members.

sible for the hydrodynamic problem). An equivalent strip-theory formula exists for the case of the BC (heave plates), as well as an adapted Morison's equation, which can the latter be found in [19]. The drag and inertia terms are computed with the Morison's equation. Drag and inertia terms related to marine growth allow for different hydrodynamic coefficients, even though that was not made due to insufficient data. The Morison's-only approach used computes buoyancy changes due to platform movements using a linearized model [13, 19]. Therefore, FAST computes the total load on the foundation from linear hydrostatics, F_i^{hidr}, according to the equation 4, written in Einstein's notation:

$$F_i^{hidr}(q) = \rho g V_0 \delta_{i3} - C_{ij}^{hidr} q_j \tag{4}$$

where ρ is the fluid's density, g is the gravitational acceleration, V_0 is the displaced volume of fluid when the platform is in its undisplaced position, δ_{i3} is the $(i, 3)$ component of the Kronecker-Delta function (i.e. identity matrix), $C_{i,j}^{hidr}$ is the (i, j) component of the linear hydrostatic restoring matrix at the centre of buoyancy, and q_j is the j^{th} platform DOF[2] [19]. The original foundation has the following hydrostatic restoring matrix:

$$\begin{aligned} C_{3,3}^{hidr} &= 3.836 \times 10^6 \ \ \mathrm{N\,m^{-1}} \\ C_{4,4}^{hidr} &= 1.074 \times 10^9 \ \ \mathrm{N\,m\,rad^{-1}} \\ C_{5,5}^{hidr} &= 1.074 \times 10^9 \ \ \mathrm{N\,m\,rad^{-1}} \end{aligned} \tag{5}$$

For all other values of the indices i, j, $C_{ij}^{hidr} = 0$.

2.3. Aerodynamic loads

FAST's Aerodyn module computes the aerodynamic loads with the Blade Element Method [16], one of the most used methods for stationary flows. As the real flow is not stationary, Aerodyn uses some corrective measures to include some important unsteady flow effects, like the stall phenomenon and vortex shedding [8, 16].

2.4. Mooring system loads

MoorDyn module is used to model the mooring system, since it accounts for non-linear mooring dynamics. The model uses finite elements, and it considers mooring lines inertia, stiffness, internal damping, buoyancy, hydrodynamic inertia and drag loads, and soil interaction. It does not account for bending stiffness of the lines. A detailed description of this model can be found in Ref. [7].

2.5. Design load case 1.1

GL guideline for offshore wind turbines [1] requires the study of various DLC to guarantee their certification, which the external conditions have to be chosen according to a specific installation site. For a first approach, it has been considered only DLC 1.1. The site chosen was the same of Ref. [11]. Table 2 presents the external conditions for the cases analysed.

Table 2: External conditions for DLC 1.1 cases analysed. $\overline{u}$ is the mean wind velocity at hub hight, H_s the significant wave height, and T_p the peak period of the sea state.

Case	$\overline{u}$ [m s^{-1}]	H_s [m]	T_p [s]
1	11.4	2.466	13.159
2	18.0	4.005	14.129
3	24.0	5.585	16.162

TurbSym was used to create the wind fields needed for the analysis with IEC Kaimal spectra and NTM (Normal Turbulence Model), see Refs. [9, 18]. Airy model with Pierson-Moscowitz spectral density was chosen to model the wave conditions, see Ref. [13]. Wind induced sea superficial currents were also considered according to IEC 61400-3 standard [9].

As mentioned before, due to the Morison's equation approach limitations, only severe wave conditions were considered. They correlate to higher wind speeds, and for this reason, only external conditions from rated to cut-out wind speeds were taken into account.

3 IMPLEMENTATION

3.1. FAST outputs

Because hydrodynamic loads decay exponentially with depth [13], the DeepCwind semisubmersible was discretized through an imaginary horizontal plane 3 meters below the SWL (sea water level). All the members intercepted by this plane were divided in two parts, see figure 2.

Three nodes on each part of the members were defined to output the distributed hydrodynamic loads applied along the length of the member. This means that the divided members have 5 nodes, as the middle one is shared by both parts, while undivided members have only three nodes. At all nodes, equation 3 is applied to compute the total hydrodynamic distributed load on each node, except for the distributed buoyancy load contribution (as mentioned in section 2.2 and to be discussed later). Once the total hydrodynamic load at each node is know, the average distributed load on the member's part is found. By acknowledging the average of the total distributed hydrodynamic load applied along the length of the part, it can be converted to the total pressure on the wet surface of the part, P^p, simply dividing it by the part's diameter. This procedure was made for the directions x, y and z, indepen-

[2] subscripts i and j range from 1 to 6, one for each platform DOF (1 = surge, 2 = sway, 3 = heave, 4 = roll, 5 = pitch, 6 = yaw)

dently. The equation is as follows:

$$P^p = \frac{\frac{1}{3}\sum_{N=1}^{3} F_N^p}{\pi D^N} \tag{6}$$

where the F_N^p is the total distributed hydrodynamic load on node N of part p, D^N the diameter at node N. $N = (1, 2, 3)$ corresponding to each one of the nodes of a member's part.

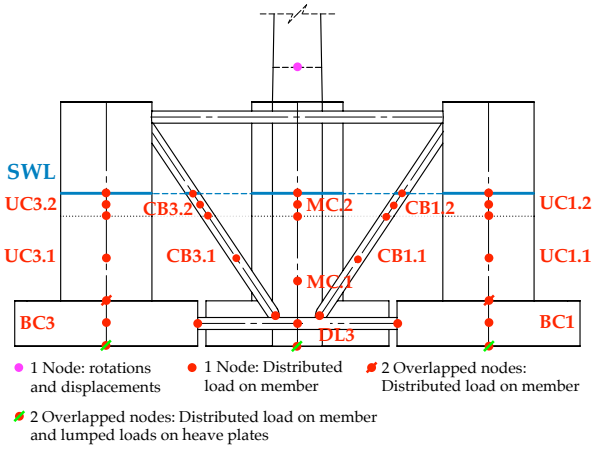

Figure 2: DeepCwind semisubmersible discretized for FAST's output definition. Behind members and their nodes are not shown.

An analogue procedure was used for the heave plates lumped loads, where they were also converted to pressure applied on their bottom faces. The total lumped loads at each heave plate node had to be determined before being converted to pressure. For this case of pressure conversion, since the lumped load is a point load, it had to be divided by its area of application. The equation is as follows:

$$P^J = \frac{F^J}{\frac{\pi}{4}(D^J)^2} \tag{7}$$

where J is the heave plate, P^J the pressure applying on the bottom face of the heave plate, F_J the total hydrodynamic lumped load on heave plate J node, and D^J the diameter of heave plate J. This process was also done independently for each direction, (x, y, z). The conversion precess from distributed loads/lumped loads to pressure took place for every time step computed with FAST. These pressures were applied on the FEM model.

3.2. FEM

The DLC 1.1 prescribes 10 minutes (600 seconds) simulations for each case with safety factor (SF) above 1.1 for their validity. As presented in Ref. [17], submodels of the welded joints were made using solid elements in order to obtain a more accurate and detail prediction of the stresses, believed to be stress concentration regions. As the FEM transient structural analysis have high computational cost, submodeling techniques were used to reduce it while keeping the required accuracy. Submodeling techniques require two models, a coarse model of the global problem and a detailed model of regions where greater refinement and detail are needed, such as stress concentration regions. This technique is based on the Saint-Venant principle and a detailed description of the method can be found in Refs. [2, 3, 15, 17]. Submodels were created on areas where the pontoons join with other members, see figure 3.

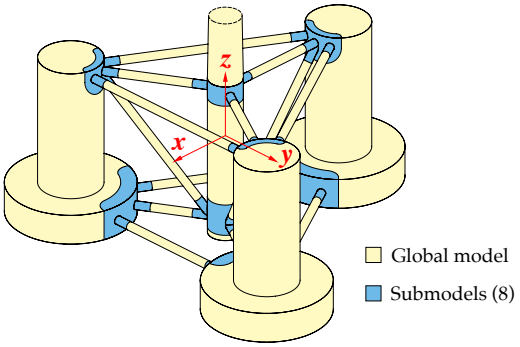

Figure 3: Global model and submodels.

3.2.1 Global model

A shell model of the semisubmersible foundation was made. On this model all the loads were applied after their preprocessing (conversion to pressure) as well as the loads of the mooring system on the semisubmersible's fairleads and the loads due to the hydrostatic restoring (existent if the platform was in any other position than the undisplaced position). As buoyancy effects were not accounted with the Morison's-only approach, hydrostatic pressure was applied to the outside surfaces of the foundation due to its draft and also on ballasts of the UCs and BCs on their interior surfaces, since buoyancy is a consequence of the hydrostatic pressure gradient along z. The global model was constrained imposing the respective displacements and rotations on the lower section of the tower, obtained with FAST, see figure 2.

3.2.2 Submodels

Submodels using solid elements were created on members joints. On the submodels' cut boundaries the displacements of the global model solution were applied. Fillets were modelled on the member unions. GL standard [1] recommends their radius to be equal to the connecting member thickness.

3.3. Analysis methodology

The original DeepCwind semisubmersible cannot stand the loads applied on it. Actually, the hydrostatic pressure on the BC alone is sufficient to make them yield. Consequently, an analysis methodology had to be created so that an adequate reinforcement of the structure could be made. To expedite the it-

erative reinforcement process, transient structural analyses were only to be considered once a semisubmersible geometry could validate ($SF > 1.1$) a static structural analysis for a random timestep (of the whole 600 s). Until it did not validate the static analysis, improvements would be done to the geometry. Once a geometry was found valid for the static analysis, it would be subjected to transient structural analysis. If the geometry could not validate the transient structural analysis, further improvements had to be made. Once a geometry verifies all the three cases presented in table 2, it is considered as a valid geometry, capable of standing the loads for normal operation. Figure 4 resumes the followed methodology for the reinforcement iterative process.

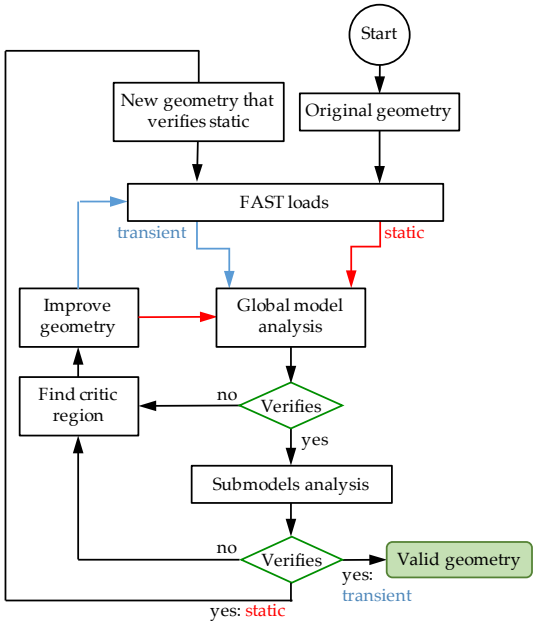

Figure 4: Flowchart resuming the methodology for the reinforcement iterative process.

4 STRUCTURAL ANALYSIS

4.1. Original DeepCwind Results

For the static structural analysis the stresses were well above the yield strength of 355 MPa, in agreement with the GL guideline [1]. See figure 5.

4.2. BC reinforcement

It can be seen that the BC cannot withstand the hydrostatic pressure applied on them. Its thickness increase was not sufficient, so internal stiffeners were studied, see figure 6.

The final concept for the BC can stand the hydrostatic pressure, as seen in figure 7.

4.3. Wall thickness increase

Although BC and UP wall thicknesses had already been increased, from figure 5 it is observed that also the pontoons and the MC would need to see their thicknesses increased. An iterative process

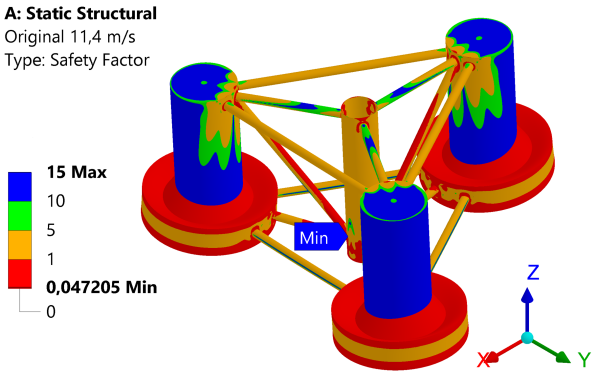

Figure 5: SF plot for 11.4 $\mathrm{m\,s^{-1}}$ static structural analysis.

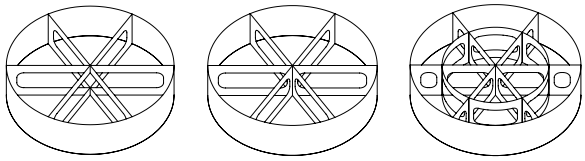

(a) Early concept. (b) Mid concept. (c) Final concept.

Figure 6: BC internal stiffeners concept evolution. BC final wall thickness 120 mm, stiffeners final thickness 100 mm. BC top cap not shown for the sake of visibility.

was initiated. As the thickness increased, the fillets' radius existent on the member unions also increased. ASM Industries, a reference industry on offshore structures, works with thicknesses up to 150 mm, a value that was assumed to be an industry limit. On the other hand, weight considerations were also taken in mind, so the limit was defined to 120 mm. For the pontoons, a 50 mm limit was chosen in order to avoid calendering problems due to their relatively small diameter. After the iterative process, the thicknesses of the BC, UP and pontoons were on the limit. Nevertheless, for the MC, it was found that further thickness increase (above 100 mm) had little to no effect on the maximum stress on the structure (located on the connection between the YU and the MC). A summary of the final thicknesses obtained from the iterative process is on table 3.

Table 3: Summary of wall thickness increase for all the DeepCwind members.

Member	Original thickness [mm]	Final thickness [mm]
MC	30	100
UC	60	120
BC	60	120
Pontoons	17.5	50

A static analysis for the semisubmersible with the BCs reinforced and member thicknesses as presented in table 3 was made. The resultant maximum equivalent stresses were $\sigma_{max} = 140.91$ MPa

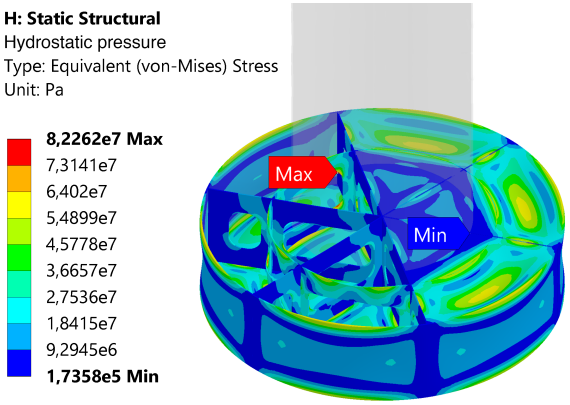

Figure 7: Stresses on BC for final concept when hydrostatic due to ballasting and draft is applied. Left half of BC top cap invisible to show inside stress distribution.

and $\sigma_{max} = 213.41\,\text{MPa}$, on the global model and top MC submodel, respectively. This means $SF = 1.66(\geqslant 1.1)$, validating the geometry for this analysis. Figure 8 shows the stress distribution of the analysis on the top MC submodel, where the maximum stresses were found.

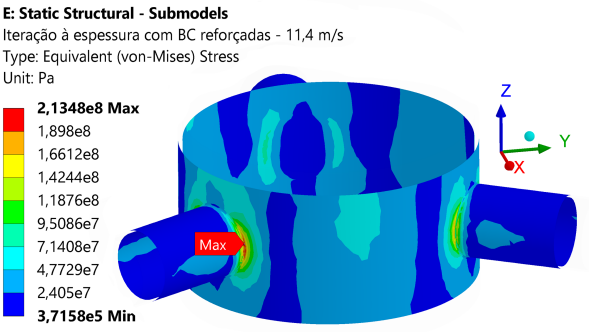

Figure 8: Stress distribution of the structural analysis on the upper MC submodel, where the maximum stresses were found.

4.3.1 MC internal reinforcement

Transient structural analysis were made starting with case 1 ($\overline{u} = 11.4\,\text{m}\,\text{s}^{-1}$)[3]. As transient structural analysis account for dynamic inertial loads, higher stresses for most of the cases are expected. For the global model analysis, the maximum stress $\sigma_{max} = 681.23\,\text{MPa}$ was found at $t = 511\,\text{s}$ on the connection of the YU with the MC ($SF = 0.52$), see figure 9. Not only on the top MC region but also on the connection of the YL and CB to the bottom region of the MC, the structure could not withstand the subjected loads. Here the maximum stress was $\sigma_{max} = 391.79\,\text{MPa}$ at $t = 505\,\text{s}$ ($SF = 0.91$). The geometry could not verify the transient structural analysis, thus requiring further geometry iterations.

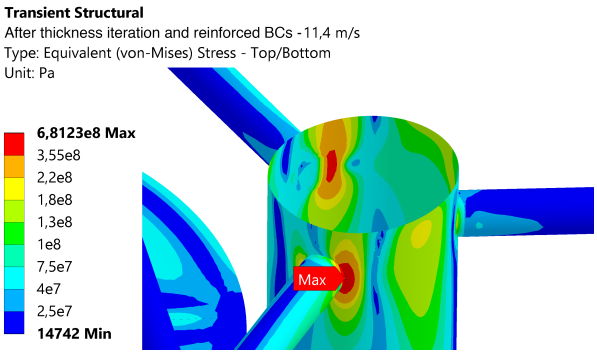

Figure 9: Stress distribution of the structural analysis on the top MC submodel, where the maximum stresses were found.

As the MC could not stand the loads on it applied, internal annular reinforcements were considered, on both top and bottom regions of the MC, where the YU and YL respectively connect. The first concept consisted on a single annular reinforcement, aligned with the centre of YL/YU. These reinforcement concept was found to be insufficient. Two additional annular reinforcements were considered both on top and bottom regions of the MC. This reinforcements were introduced with an offset of half the diameter of the YU/YL, from the existing annular reinforcement, see figure 10.

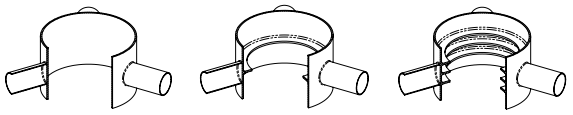

(a) No annular reinforcement. (b) One annular reinforcement. (c) Three annular reinforcements.

Figure 10: Half-cut view of upper submodel of MC and its reinforcement concept evolution. Analogous reinforcements were considered on the bottom of the MC.

No further modifications to the geometry were considered.

4.4. Final transient structural analysis

For the 3 cases presented on table 2, transient structural analysis were performed, each with different random seed (to assure different wind and wave time series between analysis). 800 s simulations were run to avoid initial numerical convergence phenomena, hence evaluating only the last 600 s.

Due to the geometry changes, the foundation's properties inevitably changed. The new CM location was found, as well as the new foundation inertias. Also, the ballasts had to be adjusted to keep the same draft and the new hydrostatic restoring matrix had to be computed. See tables 4, 5 and 6.

Case 1 maximum equivalent (von Mises) stresses on both the global model and submodels are presented in figure 11. The maximum stress over time was $\sigma_{max} = 225.76\,\text{MPa}$ at $t = 481\,\text{s}$, located on the upper MC submodel at the union between the YU and the MC.

[3]The new mass properties of the foundation were found and changed in FAST to compute the new loads applying on in (new CM location, ballasts adjusted to keep same draft, and computed the new hydrostatic restoring matrix). Although, these properties will only be presented for the final geometry analysed.

Table 4: Foundation's mass properties considering ballasting

Properties	Original	Final
Steel mass	3.8522E+6 kg	9.1882E+6 kg
Total mass	1.3473E+7 kg	1.3473E+7 kg
CM below SWL	13.46 m	12.13 m
Roll inertia	6.827E+9 kg m^{-2}	6.836E+9 kg m^{-2}
Pitch inertia	6.827E+9 kg m^{-2}	6.836E+9 kg m^{-2}
Yaw inertia	1.226E+10 kg m^{-2}	1.116E+10 kg m^{-2}

Table 5: Ballasting properties.

Properties	Original	Final
Height at UC	7.830 m	- m
Height at BC	5.048 m	3.196 m
Total mass	9.621E+6 kg	4.285E+6 kg

Table 6: Hydrostatic restoring matrix. Entries not shown are zero.

Properties	Original	Final
$C^{hidr}_{3,3}$	3,836E+6 N m^{-1}	3,836E+6 N m^{-1}
$C^{hidr}_{4,4}$	1,074E+9 N m rad^{-1}	1,702E+9 N m rad^{-1}
$C^{hidr}_{5,5}$	1,074E+9 N m rad^{-1}	1,702E+9 N m rad^{-1}

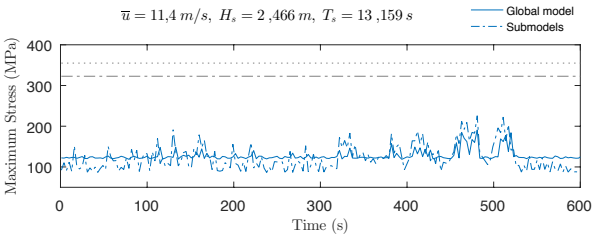

Figure 11: von Mises maximum stresses over time for case 1, for the global model and submodels.

For case 2, the maximum stress over time $\sigma_{max} = 342.86$ MPa was also located on the union between the YU and the MC, at $t = 169$ s. This corresponds to a minimum safety factor over time of 1.035, bellow the minimum limit of 1.1 stated by the GL standard [1]. For this reason, this geometry is not capable of verifying the normative conditions.

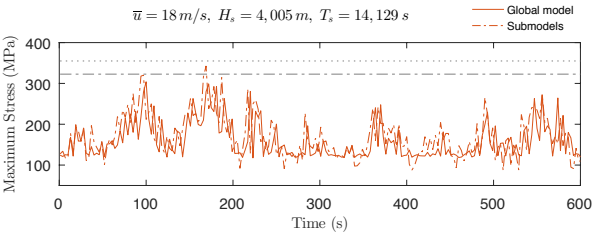

Figure 12: von Mises maximum stresses over time for case 2, for the global model and submodels.

The analysis for case 3 presented higher maximum stresses over time, going up to $\sigma_{max} = 378.63$ MPa at $t = 292$ s, above the yield stress stated by the GL standard [1], of 355 MPa, which means a minimum safety factor of $SF = 0.94$ over time. This stress was located also at the connection of the YU with the MC. The yield region can be seen in figure 14.

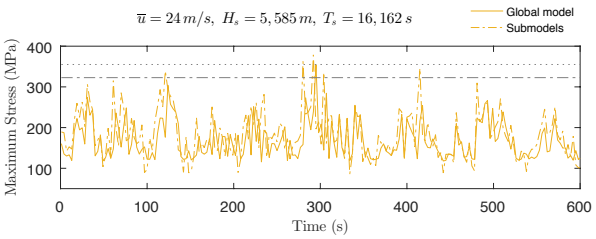

Figure 13: von Mises maximum stresses over time for case 3, for the global model and submodels.

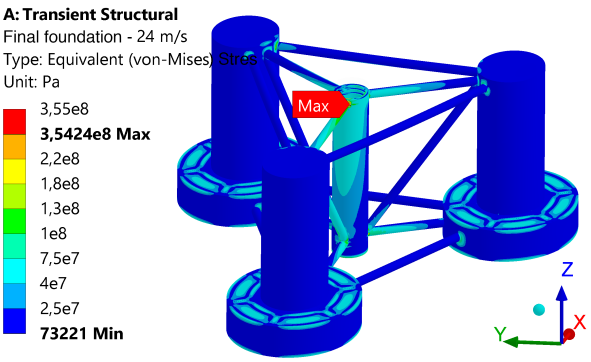

(a) Global model.

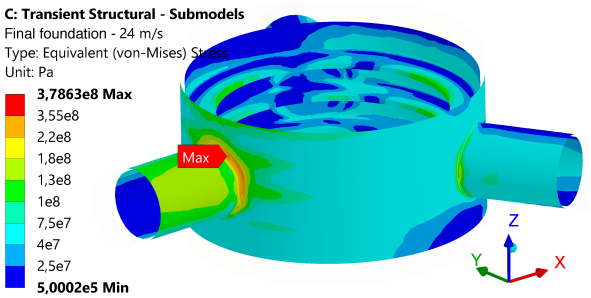

(b) Upper MC submodel.

Figure 14: Stress distribution for time of von Mises maximum stresses on case 3.

The maximum stresses tend to increase with the increase of wind speed $\overline{u}$, and therefore the increase of the significant wave height H_s and peak period T_p. The main reason why this happens may be due to the inertial loads accounted by the transient structural analysis. The inertial loads may depend mainly on the H_s and T_p, since they have a bigger influence on the structure's acceleration. Although, analysis have to be made for increasing H_s and T_p while $\overline{u}$ is kept constant, to attest this hypothesis.

4.5. Modal analysis

Despite the final geometry analysed not being capable of standing the loads, it may be close to accomplish it with some adjustments. Thus, a free-free modal analysis was performed of the final foundation considered, whose the results may be somehow representative of a geometry that verifies the tran-

sient structural analysis. These analysis were made considering every ballast as a point-mass with the respective properties. Alike, the rotor+nacelle assembly was represented by a point-mass with its inertial properties. On table 7, the first natural frequencies of the final structure are compared with the frequencies of the original one.

Table 7: Structure's natural frequencies

Mode description	Frequency [Hz]	
	Original	Final
1st Tower Side-to-Side	0.2843	0.3094
1st Tower Fore-Aft	0.2854	0.3096
1st Tower Torsion	03659	0.7456
2nd Tower Side-to-Side	0.5540	1.7327
2nd Tower Fore-Aft	0.5544	1.7564
3rd Tower Side-to-Side	1.3468	4.7055
3rd Tower Fore-Aft	1.4442	4.7127

According to Arany et al. [4], the main dynamic loads acting on the structure are turbulent wind, wave loads that depend from their H_s and T_p, 1P loads due to the imbalances of the rotor, and 3P loads due to shadowing effects of the blades passing in front of the tower. Indeed, 1P and 3P are frequency bands, because they depend on the rotational speed of the rotor, which is of variable-speed. 1P band corresponds to the rotor rotation frequency, and 3P is three times the rotor rotation frequency, since the NREL 5 MW Reference wind turbine is three-bladed. There are three types of possible designs from the first natural frequency (f_0) of the tower point of view [4]:

1. *Soft-soft* if f_0 is below the 1P band;
2. *Soft-stiff* if f_0 is between the 1P and 3P band;
3. *Stiff-stiff* if f_0 is above the 3P band.

The GL standard [1] also states that the f_0 should not be placed within 10% of the 1P and 3P bands. For this turbine, which operates from 6.9 rpm to 12.1 rpm, the P1 and P3 bands, considering the 10% offset, are $[0.1035; 0.2218]$ Hz and $[0.9315; 1.997]$ Hz, respectively. Thus, f_0 is between 1P and 3P respecting the 10% condition. Besides, the wave load frequencies are comprised between 0.05 and 0.167 Hz, for the site considered (the same as in Ref. [11]). Therefore, since f_0 is above the wave loads frequency and between 1P and 3P bands, respecting the 10% condition, the final geometry is a possible design. Notwithstanding, an analysis of the wind turbulence must also be made as well as loads from eddies generated downstream of the tower and blades.

4.6. Response analysis

As the foundation properties changed, so did its hydrodynamic response. For this analysis was considered no wind and still water. The wind turbine was halted with the brake engaged. Potential flow theory was used for the hydrodynamic problem, since the Morison's equation is not valid for this conditions, as explained in section 2.2. For each one of the 6 DOF of the foundation, analysis were made with an initial misalignment (whose can be seen at $t = 0$ on figure 15). The results are presented in table 8 and in figure 15.

Table 8: Structure's hydrodynamic response frequencies

DOF	Frequency [Hz]	
	Original	Final
Surge	0,009	0,009
Sway	0,009	0,009
Heave	0,058	0,058
Roll	0,039	0,041
Pitch	0,039	0,041
Yaw	0,016	0,013

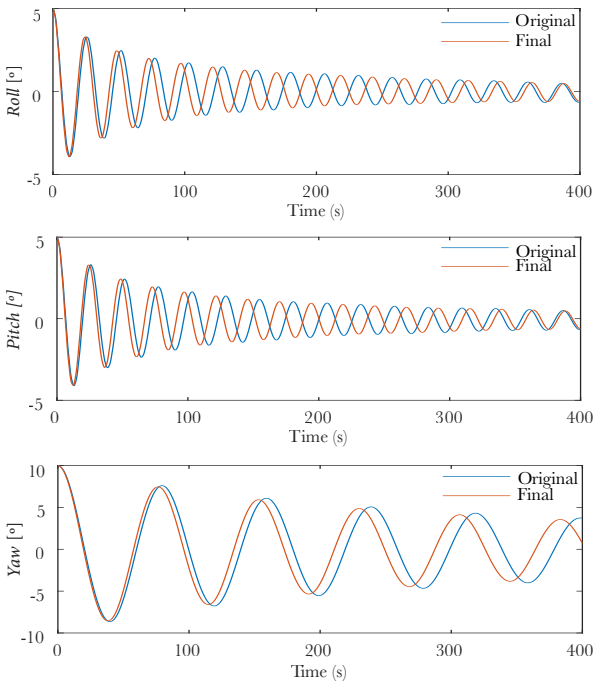

Figure 15: Hydrodynamic response comparison between the original and final foundation. Only the DOFs that changed their response are shown.

Not all DOFs changed their response. Surge and sway response depend mostly on the total mass of the structure and on the properties of the mooring lines. Since the mass of the structure and the mooring lines were unaffected, the response stayed the same. The heave response stayed the same because the hydrostatic restoring matrix coefficient $C^{hidr}_{3,3}$ also stayed the same since the water plane area was equal, as well as the total mass of the structure and the mooring lines properties. Roll and pitch response changed due to the changes in the hydrostatic restoring matrix coefficients ($C^{hidr}_{4,4}$ and $C^{hidr}_{5,5}$, respectively), the changes of the inertias of the foundation (I_{xx} and I_{yy}, respectively), and also due to the change in the CM position. The response for the yaw DOF also changed but due only to the change of the I_{zz} inertia of the foundation.

5 CONCLUSIONS

Due to the incapability of the BCs to stand the hydrostatic pressure, two possible solutions are seen as possible:

1. Internal reinforcement of the BCs, as presented on this document or with alternative concepts;
2. Replacement of the BC by heave plates, without any free interior volume, and thus not to be affected by the hydrodynamic pressure. An example are the heave plates used by the *WindFloat*.

The thickness of the overall foundation was found to be bellow the necessary for the structure to withstand the existent loads. However, with the increase of thickness, and the added internal reinforcements on the BC,, the foundation still yield on the unions of the YU with the MC. This region was considered to be the weaker region of the entire foundation. An increase in the pontoon's diameter or a reduction of the distance between the UC+BC (of the side of the triangle formed by the columns) may be a possible solution to this problem.

The maximum stresses tend to increase with the increase of wind speed $\overline{u}$, and therefore the increase of the significant wave hight H_s and peak period T_p. This is believed to be because of the inertial loads that may depend mainly on the H_s and T_p, since they have a bigger influence on the structure's movement. To attest this hypothesis, analysis have to be made for increasing H_s and T_p while $\overline{u}$ is kept constant.

REFERENCES

[1] Rules and Guidelines Industrial Services Guideline for the Certification of Offshore Wind Turbines. Standard, Germanischer Lloyd (GL), 2012.

[2] ANSYS. ANSYS advanced analysis techniques guide. *Ansys Help*, (November), 2007.

[3] ANSYS. Reduction Techniques, Part 1: Submodeling Applicability and Example, 2012.

[4] L. Arany, S. Bhattacharya, J. Macdonald, and S. J. Hogan. Simplified critical mudline bending moment spectra of offshore wind turbine support structures. *Wind Energy*, 2014.

[5] S. Butterfield, W. Musial, and J. Jonkman. Engineering Challenges for Floating Offshore Wind Turbines. 2007.

[6] J. Cruz and M. Atcheson. *Floating Offshore Wind Energy: the next generation of wind energy*. Spinger, 2016.

[7] M. Hall and A. Goupee. Validation of a lumped-mass mooring line model with DeepCwind semisubmersible model test data. *Ocean Engineering*, 104, 2015.

[8] M. O. Hansen. *Aerodynamics of Wind Turbines*. 2015.

[9] Wind turbines - Part 3: Design Requirements for Offshore Wind Turbines. Standard, International Electrotechnical Commission (IEC), 2006.

[10] J. Jonkman, S. Butterfield, W. Musial, and G. Scott. Definition of a 5-MW reference wind turbine for offshore system development. Technical report, NREL, 2009.

[11] J. M. Jonkman. Dynamics modeling and loads analysis of an offshore floating wind turbine. Technical report, NREL, 2007.

[12] J. M. Jonkman, T. Larsen, A. C. Hansen, T. Nygaard, K. Maus, M. Karimirad, Z. Gao, T. Moan, I. Fylling, J. Nichols, M. Kohlmeier, J. P. Vergara, D. Merino, W. Shi, and H. Park. Offshore code comparison collaboration within IEA Wind Task 23: Phase IV results regarding floating wind turbine modeling. Technical report, NREL, 2010.

[13] J. M. Jonkman, A. N. Robertson, and G. J. Hayman. HydroDyn User's Guide and Theory Manual HydroDyn User's Guide and Theory Manual. (March), 2015.

[14] C. Luan, Z. Gao, and T. Moan. Development and verification of a time-domain approach for determining forces and moments in structural components of floaters with an application to floating wind turbines. *Marine Structures*, 2016.

[15] E. Madenci and I. Guven. *The finite element method and applications in engineering using ANSYS*. Spinger, 2006.

[16] P. J. Moriarty and A. C. Hansen. Aerodyn theory manual. *Renewable Energy*, 2005.

[17] E. Narvydas and N. Puodziuniene. Applications of sub-modeling in structural mechanics. In *Mechanika*, 2014.

[18] N. Neil Kelley, Bonnie Jonkman. TurbSim User's Guide: Version 1.50 TurbSim User's Guide:. 2009.

[19] A. Robertson, J. Jonkman, and M. Masciola. Definition of the Semisubmersible Floating System for Phase II of OC4. *Golden, CO*, 2014.

[20] A. Robertson, J. Jonkman, F. Vorpahl, J. Qvist, and et al. Offshore code comparison collaboration, Continuation within IEA wind Task 30: Phase II results regarding a floating semisubmersible wind system. *Proceedings of the 33rd International Conference on Ocean, Offshore and Arctic Engineering (OMAE2014)*, 2014.

[21] F. Wendt, A. Robertson, J. Jonkman, and G. Hayman. Verification of New Floating Capabilities in FAST v8. *Proceedings of the AIAA SciTech*, 2015.